

Figure 1. Schematic diagram of volatile lens evaporating on the immiscible liquid surface in toroidal coordinates.

experimentally studied deionized water droplet evaporation on the structured superhydrophobic surface. They found that the droplet lifetime is longer than the theoretical value calculated by the isothermal quasi-steady model due to the influence of evaporative cooling. Xu and Ma¹⁹ described the effect of evaporative cooling on the droplet evaporation process on the surface of the solid substrate. Chandramohan et al.²⁰ experimentally studied the spatiotemporal interface temperature distribution for water droplet evaporation on a nonwetting copper substrate by using an infrared thermal imager. They found that the temperature distribution along the droplet surface is uneven due to the influence of evaporative cooling, and the temperature drop at the symmetry axis of the droplet was the largest and related to the droplet height. Nguyen et al.²¹ and Shen et al.²² deduced the analytical solutions of the temperature distribution inside the droplet and the vapor concentration distribution around the droplet with coupled boundary conditions at the gas–liquid interface established by the heat and mass transfer relationship and analyzed the influence of evaporative cooling on the droplet evaporation process on a flat solid surface²¹ and a curved solid surface.²²

Although many studies have tried to eliminate the coffee ring phenomenon and obtain a uniform pattern,²³ they can only obtain a relatively uniform macroscopic and highly disordered microscopic structure because of the inevitable roughness and heterogeneity of traditional rigid surfaces. Nowadays, more and more studies have focused on the phase transition process of droplets on immiscible liquid surfaces because they provide soft, smooth, and homogeneous surfaces. The related research is mainly experimental. Li et al.²⁴ obtained a macroscopically uniform and ordered structure on phenyl methyl silicone oil substrate. In their studies, the final deposit pattern formed due to the bending deformation of the liquid substrate and the movement of the contact line. There was no in-depth analysis from the perspective of the microfluid flow caused by droplet evaporation and contact line movement. Recently, Hakimian et al.²⁵ experimentally investigated the freezing of a few nanometer water droplets on soft interfaces. The results showed that ice formation on soft interfaces could cause interface deformation, which led to the suppression of ice nucleation as well as the freezing temperature falling below the homogenous bulk nucleation limit. Some experimental studies examined the evaporation process of a volatile droplet on another immiscible liquid substrate surface. Nosoko et al.²⁶ studied the *n*-pentane lens evaporation on a water surface using laser shadowgraphy. Sun and Yang²⁷ investigated the evaporation process of toluene and

hexane lenses on a deionized water surface. Wang and Shi²⁸ used an infrared camera to study the Marangoni convection pattern of methanol lens evaporation on the immiscible liquid surface. They found that the temperature distribution on the methanol lens surface was also uneven, and the lowest temperature was near the symmetry axis of the lens for most of the lens life.

In our previous studies,^{15–17} the evaporation processes of hexane lenses on the ionic liquid ([BMIm]PF₆) and distilled water surfaces were experimentally studied, and a theoretical model for predicting the morphology evolution of a volatile liquid lens evaporation on another immiscible liquid substrate surface was established. Considering the dynamic process of contact line motion, the diffusion-controlled evaporation model was used to calculate the mass evaporation rate. The results indicated that the calculated values of the hexane lens radius by the isothermal model are smaller than the experimental data, and the deviation increases as ionic liquid temperature rises. Based on our previous model, an improved theoretical model of the volatile liquid lenses' evaporation on another immiscible liquid substrate surface is established in the toroidal coordinate system. Using coupled boundary conditions based on the heat and mass transfer relationship at the gas–liquid interface, especially considering the evaporative cooling effect, analytical solutions of the temperature field inside the lens and the vapor concentration field around the lens are derived for the first time. This study will help to deeply understand the droplet evaporation behavior on flexible curved surfaces and provide a theoretical basis for this behavior.

THEORETICAL ANALYSIS

Theoretical Model. The evaporation of a volatile lens on the immiscible liquid surface in a toroidal coordinate system is schematically shown in Figure 1. Since the lens can be considered a combination of upper and lower spherical caps, its axisymmetric profile is described by $(0 \leq \eta < \infty, \pi - \alpha)$ and $(0 \leq \eta < \infty, \pi + \beta)$ in the toroidal coordinates (η, φ) . α and β are the angles between the upper spherical crown, the lower crown, and the horizontal plane at the contact line, respectively. r_c is the contact radius. T_∞ and C_∞ represent the temperature and vapor concentration of the ambient air at infinity, respectively. T_{sub} is the temperature of the liquid substrate. r and z refer to the radial position and axial position, respectively. \vec{i}_φ and \vec{i}_η are the unit vectors along the φ -axis and η -axis, respectively.

The theoretical model is assumed as follows: (1) since the angle between the liquid substrate and the horizontal plane at the contact line is usually small,^{15,17,29} it can be considered that

the liquid substrate–air interface remains horizontal [as described in $(0 \leq \eta < \infty, 0)$ or $(0 \leq \eta < \infty, 2\pi)$]; (2) the lens–liquid substrate interface and the liquid substrate–air interface maintain a constant temperature T_{sub} ; (3) the convection heat transfer inside the lens is negligible; and (4) since our experiment was carried out in an open environment, the lens evaporation can be simplified as a quasi-steady diffusive evaporation process,^{21,22} and thus the vapor concentration on the lens surface can be considered as the saturation concentration corresponding to the surface temperature.

Moreover, the derivations in detail can be found in the Supporting Information, and a brief introduction is given below.

The governing equations of the temperature field inside the lens and the vapor concentration field around the lens in the evaporation process can be described by $\nabla^2 T = 0$ and $\nabla^2 C = 0$, which can be transformed into the following form in the toroidal coordinate system:²²

$$\frac{\partial}{\partial \eta} \left(\frac{\sinh \eta}{\cosh \eta - \cos \varphi} \frac{\partial U}{\partial \eta} \right) + \frac{\partial}{\partial \varphi} \left(\frac{\sinh \eta}{\cosh \eta - \cos \varphi} \frac{\partial U}{\partial \varphi} \right) = 0 \quad (1)$$

where $U(\eta, \varphi) = T(\eta, \varphi) - T_{\text{sub}}$ or $U(\eta, \varphi) = C(\eta, \varphi) - C_{\infty}$ can be described as excess temperature or excess vapor concentration.

The boundary conditions of the temperature field and vapor concentration field in toroidal coordinates are as below:

For the region inside the lens ($0 \leq \eta < \infty, \pi - \alpha \leq \varphi \leq \pi + \beta$), the following conditions apply:

- (1) The lens is axially symmetric on the axis of symmetry:

$$\left. \frac{\partial T(\eta, \varphi)}{\partial \eta} \right|_{\eta=0} = 0 \quad (2)$$

- (2) At the lens–liquid substrate interface, the temperature remains constant:

$$T(\eta, \pi + \beta) = T_{\text{sub}} \quad (3)$$

- (3) At the lens–air interface, the evaporative cooling effect is considered.

$$q(\eta, \varphi)|_{\varphi=\pi-\alpha} = LJ(\eta)|_{\varphi=3\pi-\alpha} \quad (4)$$

where q , L , and J are the heat flux, the latent heat of lens vaporization, and the evaporation flux at the lens–air interface, respectively.

For the vapor region around the lens ($0 \leq \eta < \infty, 2\pi \leq \varphi \leq 3\pi - \alpha$), the following conditions apply:

- (4) The vapor region around the lens is also axially symmetric and on the axis of symmetry:

$$\left. \frac{\partial C(\eta, \varphi)}{\partial \eta} \right|_{\eta=0} = 0 \quad (5)$$

- (5) At the liquid substrate–air interface, vapor does not penetrate into the liquid substrate:

$$\left. \frac{\partial C(\eta, \varphi)}{\partial \varphi} \right|_{\varphi=2\pi} = 0 \quad (6)$$

According to Nguyen et al.²¹ and Shen et al.,²² the variable separation method is used to solve eq 1 with coupled boundary conditions (eqs 2–6). The normalized temperature distribution inside the lens and the normalized vapor concentration distribution around the lens can be obtained as follows:

$$\tilde{T}(\eta, \varphi) = \frac{T(\eta, \varphi) - T_{\text{sub}}}{T_{\text{sub}} - T_{\infty}} = \sqrt{2(\cosh \eta - \cos \varphi)} \times \int_0^{\infty} E_T(\tau) P_{\text{ir}-0.5}(\cosh \eta) \sinh[(\pi + \beta - \varphi)\tau] d\tau \quad (7)$$

$$\tilde{C}(\eta, \varphi) = \frac{C(\eta, \varphi) - C_{\infty}}{C_e - C_{\infty}} = \sqrt{2(\cosh \eta - \cos \varphi)} \times \int_0^{\infty} E_C(\tau) P_{\text{ir}-0.5}(\cosh \eta) \cosh[(2\pi - \varphi)\tau] d\tau \quad (8)$$

where $P_{\text{ir}-0.5}(\cosh \eta) = \frac{1}{\pi} \int_0^{\pi} \frac{1}{(\cosh \eta + \sinh \eta \cos x)^{0.5+ir}} dx$ is the Legendre function of the first kind,³⁰ τ refers to the integration dummy, and C_e is the saturated vapor concentration of the lens at T_{sub} . $E_T(\tau)$ and $E_C(\tau)$ are functions of the integration dummy that are independent of η and φ :

$$E_T(\tau) = \frac{\cosh(\alpha\tau)}{\sinh[(\alpha + \beta)\tau] \cosh(\pi\tau)} \times E_0 \left\{ \tau F(\alpha, \tau) \tanh[(\alpha - \pi)\tau] - \frac{1}{3} \frac{dF(\alpha, \tau)}{d\alpha} \right\} / \left\{ \tau F(\alpha, \tau) \coth[(\alpha + \beta)\tau] - \frac{1}{3} \frac{dF(\alpha, \tau)}{d\alpha} \right\} - E_0 \left\{ \tau F(\alpha, \tau) \tanh[(\alpha - \pi)\tau] - \frac{1}{3} \frac{dF(\alpha, \tau)}{d\alpha} \right\} \quad (9)$$

$$E_C(\tau) = \frac{\cosh(\alpha\tau)}{\cosh[(\alpha - \pi)\tau] \cosh(\pi\tau)} \times \left\{ \tau F(\alpha, \tau) \coth[(\alpha + \beta)\tau] - \frac{1}{3} \frac{dF(\alpha, \tau)}{d\alpha} \right\} / \left\{ \tau F(\alpha, \tau) \coth[(\alpha + \beta)\tau] - \frac{1}{3} \frac{dF(\alpha, \tau)}{d\alpha} \right\} - E_0 \left\{ \tau F(\alpha, \tau) \tanh[(\alpha - \pi)\tau] - \frac{1}{3} \frac{dF(\alpha, \tau)}{d\alpha} \right\} \quad (10)$$

where the evaporative cooling number E_0 and the thermal gradient of vapor saturation concentration with temperature b are defined as $E_0 = bLD/k$ and $b = dC_{\text{sat}}/dT$, respectively.^{21,22} And D is the diffusion coefficient, k is the thermal conductivity of the lens, and $F(\alpha, \tau)$ can be calculated as follows:

$$F(\alpha, \tau) = 2\sqrt{2} \frac{\sinh(\alpha\tau)}{\sinh(\pi\tau) \sin \alpha} \quad (11)$$

The heat flux q at the lens–air interface can be calculated by the following formula:

$$q(\eta, \pi - \alpha) = \frac{T_{\text{sub}} - T_{\infty}}{r_c/k} \sqrt{2} (\cosh \eta + \cos \alpha)^{3/2} \times \int_0^{\infty} E_T(\tau) P_{ir-0.5}(\cosh \eta) \left\{ \frac{\sin \alpha \sinh[(\alpha + \beta)\tau]}{2(\cosh \eta + \cos \alpha)} - \tau \cosh[(\alpha + \beta)\tau] \right\} d\tau \quad (12)$$

The evaporation flux at the lens–air interface can be calculated as follows:

$$J(\eta) = \frac{C_e - C_{\infty}}{r_c/D} \sqrt{2} (\cosh \eta + \cos \alpha)^{3/2} \times \int_0^{\infty} E_C(\tau) P_{ir-0.5}(\cosh \eta) \left\{ \frac{\sin \alpha \cosh[(\alpha - \pi)\tau]}{2(\cosh \eta + \cos \alpha)} - \tau \sinh[(\alpha - \pi)\tau] \right\} d\tau \quad (13)$$

The lens mass evaporation rate can be obtained by integrating eq 13 over the lens surface.

$$\begin{aligned} \frac{dm}{dt} &= \int_0^{\infty} 2\pi r_c^2 J(\eta) \frac{\sinh \eta}{(\cosh \eta + \cos \alpha)^2} d\eta \\ &= 2\sqrt{2} \pi r_c D (C_e - C_{\infty}) \times \int_0^{\infty} d\tau \\ &\quad \int_0^{\infty} \frac{\sinh \eta}{\sqrt{\cosh \eta + \cos \alpha}} E_C(\tau) P_{ir-0.5}(\cosh \eta) \\ &\quad \left\{ \frac{\sin \alpha \cosh[(\alpha - \pi)\tau]}{2(\cosh \eta + \cos \alpha)} - \tau \sinh[(\alpha - \pi)\tau] \right\} d\eta \end{aligned} \quad (14)$$

Note that in our previous research,¹⁷ a theoretical model of the morphological evolution of volatile liquid lenses on the immiscible liquid surface was introduced, so this explanation will not be repeated in this paper. Based on the previous model, the coupled heat and mass transfer process is highlighted in this paper.

RESULTS AND DISCUSSION

Validation of the Theoretical Model. A recent experimental study showed that the temperature distribution on the lens surface is not uniform.²⁸ This is similar to the sessile droplet evaporation on the surface of solid substrates. Our previous research also showed that the change in calculated lens radius under the constant temperature assumption was smaller than the experimental data, and the deviation increases as the liquid substrate temperature rises (as shown by the dotted line in Figures 2 and 3).¹⁷ Consequently, it is significant to consider the interfacial evaporative cooling effect in the theoretical study of lens evaporation on the liquid substrate surface, especially on a heated liquid substrate surface. To demonstrate the reliability of the analytical model established based on the interfacial cooling effect, the experimental data for hexane lens evaporation on an ionic liquid ([BMIm]PF₆) substrate with a depth of 4 mm was used as a comparison. The ambient temperature during the experiment was 15 °C, and the spreading stage was ignored

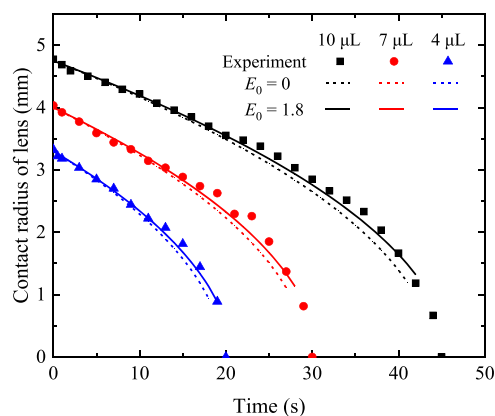


Figure 2. Comparison of change in contact radius for different initial hexane lens volumes between calculated results and experimental data when the ionic liquid temperature is 16 °C.

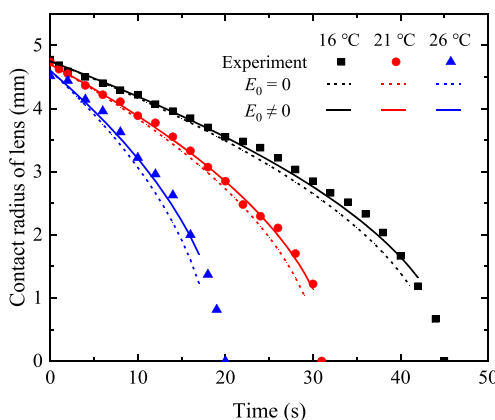


Figure 3. Comparison of change in contact radius for different ionic liquid temperatures between calculated results and experimental data when initial hexane lens volume is 10 μL.

in the model calculation because the ratio of the spreading stage to the lens lifetime was small. Figures 2 and 3 compare the lens contact radius calculated by the present model and the isothermal model with the experimental data. The evaporative cooling number E_0 represents the influence of evaporative cooling on the lens mass evaporation rate. When $E_0 = 0$, the theoretical model in this study is transformed into an isothermal model. The lens mass evaporation rate calculated by eq 14 is roughly equal to that calculated by Picknett and Bexon.⁷ With increasing liquid substrate temperature, the evaporative cooling number E_0 increases, which means the evaporative cooling effect has a greater impact on lens evaporation. As can be seen from Figures 2 and 3, compared with the isothermal model, the change in lens contact radius calculated by the present model, which considers the influence of evaporative cooling over time, is more consistent with the experimental data, especially when the liquid substrate temperature is higher (as shown in Figure 3, when the substrate temperature is 26 °C).

Figure 4 shows the excess temperature field (i.e., the real temperature minus the liquid substrate temperature) inside the hexane lens when the ionic liquid temperatures are 16, 21, and 26 °C, respectively. The time shown in the figure is when the lens is spread to the maximum contact diameter. When the temperature of ionic liquid is 16, 21, and 26 °C, the initial values of contact angles α and β are 3.47° and 3.24°, 3.66° and

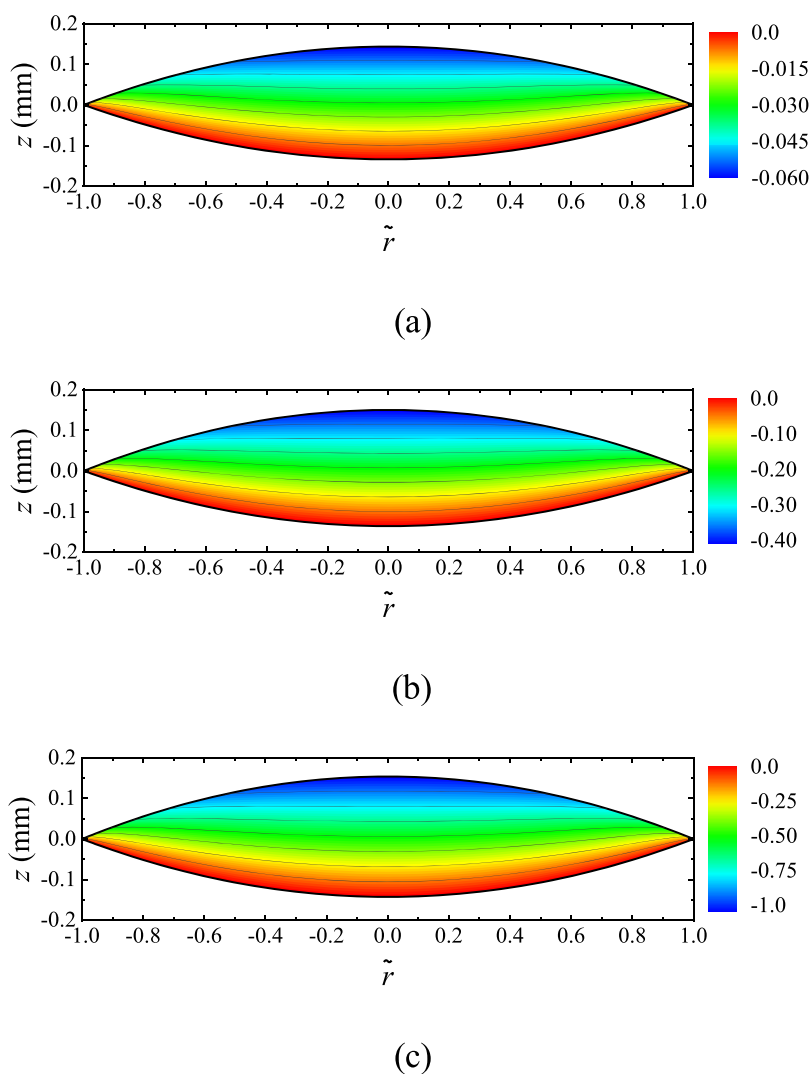


Figure 4. The temperature field inside a hexane lens when the ionic liquid temperature is (a) 16 °C, (b) 21 °C, and (c) 26 °C (initial hexane lens volume of 10 μL).

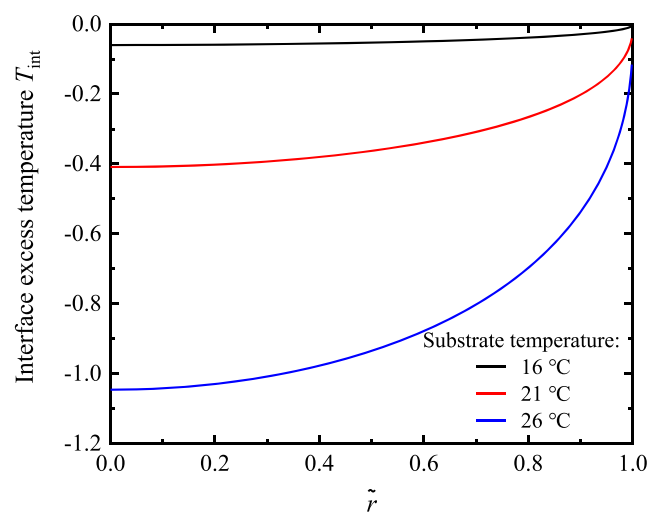
3.32°, 3.84° and 3.56°, respectively. The excess temperature distribution inside the lens is also uneven, and the lowest temperature appears on the symmetry axis of the lens surface. This is similar to the infrared image obtained by Wang and Shi,²⁸ which recorded the surface temperature distribution of methanol lens evaporation on the liquid substrate surface. The reason for the calculation results shown in Figure 4 is that the heat conduction distance between the lens–liquid interface and the lens–air interface decreases monotonously in the radial direction. In other words, the higher the lens, the lower the minimum temperature of the lens surface.

Figure 5 shows the radial variation of the interface excess temperature and heat flux along the lens–air interface at different ionic liquid temperatures when the initial hexane lens volume is 10 μL . The excess temperature and heat flux at the lens–air interface increase monotonically from the lens center to the contact line. With the increase of ionic liquid temperature, the excess temperature decreases and the heat flux increases at the lens–air interfacial center. According to Fourier’s law, the thermal resistance between the lens–liquid interface and the lens–air interface also decreases monotonically in the radial direction.

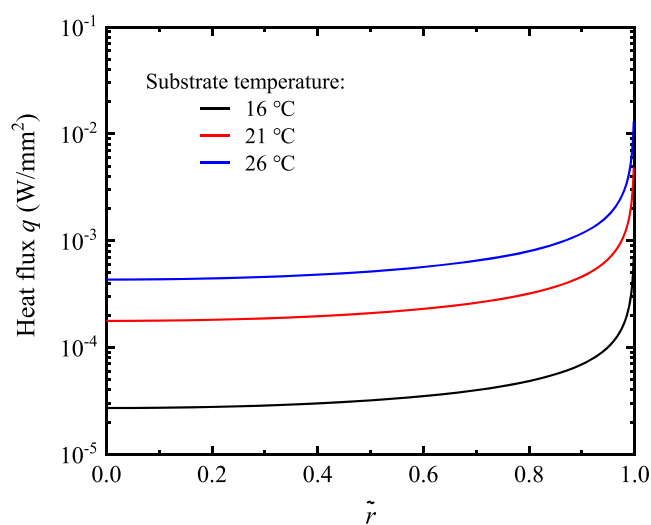
When a sessile droplet evaporates on a solid substrate, the evaporation flux distribution along the droplet surface can be well approximated by the following formula given by Deegan et al.⁹

$$J(r) = J_0(1 - \tilde{r}^2)^{-\lambda(\alpha)} \quad (15)$$

where $\lambda(\alpha) = \frac{1}{2} - \frac{\alpha}{\pi}$ represents the evaporation uniformity and J_0 is the evaporation flux at the symmetry axis of the lens surface. Figure 6 compares the evaporation flux distribution along the lens–air interface calculated by eq 13 and that calculated by eq 15 at different ionic liquid temperatures when the initial hexane lens volume is 10 μL . Equation 15 roughly describes the evaporation flux distribution along the lens surface. The deviation increases as the liquid temperature rises along the radial direction. At $\tilde{r} = 0.8$, the deviations are 5.57, 6.24, and 8.34% when the ionic liquid temperature is 16, 21, and 26 °C, respectively. The main reason for the deviation is that compared with the sessile droplet evaporation on a solid substrate surface, the heat conduction distance between the lens–liquid interface and the lens–air interface decreases faster near the contact line (as shown in Figure 4). Note that the evaporation flux along the lens surface also increases



(a)



(b)

Figure 5. Radial variation of (a) interface excess temperature and (b) heat flux along lens surface for different ionic liquid temperatures when initial hexane lens volume is $10 \mu\text{L}$.

monotonically from the lens center to the contact line, especially near the contact line.

Effect of the Density Ratio. According to our previous study,¹⁷ the density ratio of the lens to the substrate ($\rho_{\text{lens}}/\rho_{\text{substrate}}$) has an influence on the lens shape and then on its evaporation rate. Figure 7a shows the variation of excess temperature at the lens surface center and mass evaporation rate with density ratio when the ionic liquid temperature is $21 \text{ }^\circ\text{C}$. To avoid other effects on the lens evaporation process, the density ratio is adjusted only by changing the substrate liquid density to transform the morphology of lens evaporation on another immiscible liquid substrate surface. When the density ratio changes from 0.1 to 1.1, the lens is heavier relative to the substrate liquid, the lens shape changes from A to B gradually (as shown in Figure 7b), that is, α decreases and β increases monotonically with increasing density ratio. The influence of

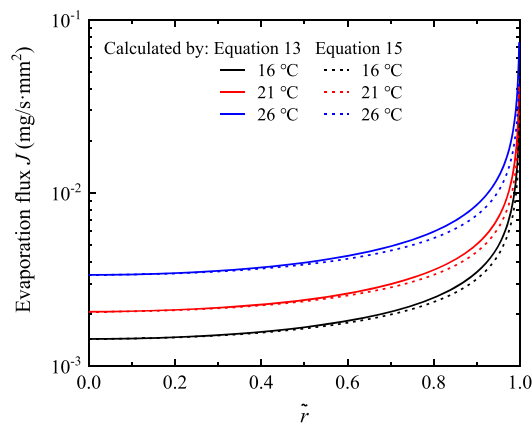
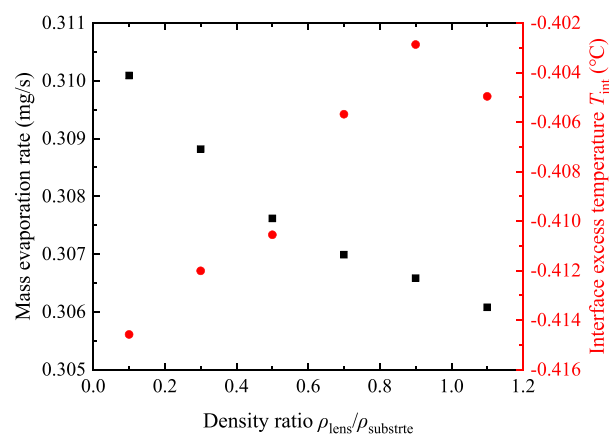
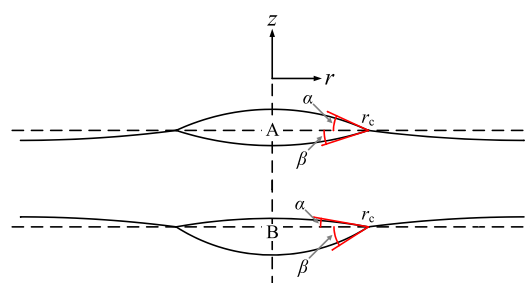


Figure 6. Comparison of lens surface evaporation flux distribution at different ionic liquid temperatures calculated according to eq 13 and 15 when initial hexane lens volume is $10 \mu\text{L}$.



(a)



(b)

Figure 7. (a) Variation of excess temperature at lens surface center and mass evaporation rate with density ratio when the ionic liquid temperature is $21 \text{ }^\circ\text{C}$ and (b) schematic diagram for shapes of volatile lens evaporation on the immiscible liquid substrate.

density ratio on mass evaporation rate and interface excess temperature is shown in Figure 7a.

The mass evaporation rate is mainly related to the value of α . As the density ratio increases, α decreases, resulting in the decrease of the area of the upper interface of the lens, that is, the effective evaporation area decreases, so the mass evaporation rate decreases. This is consistent with our previous experimental observation¹⁶ that the lens evaporation time was significantly prolonged when the lens created a “pit” in the liquid substrate.

The interface excess temperature is related to the heat conduction distance between the lens–liquid substrate interface and the lens–air interface at the symmetry axis, that is the angle of $\alpha + \beta$ is the main reason affecting the interface excess temperature. With the increase of density ratio, the angle of $\alpha + \beta$ first decreases and then increases, resulting in the temperature difference between the lens top and the substrate decreases first and then increases.

Effect of Evaporative Cooling. Figure 8 shows the variation of excess temperature at the lens surface center and

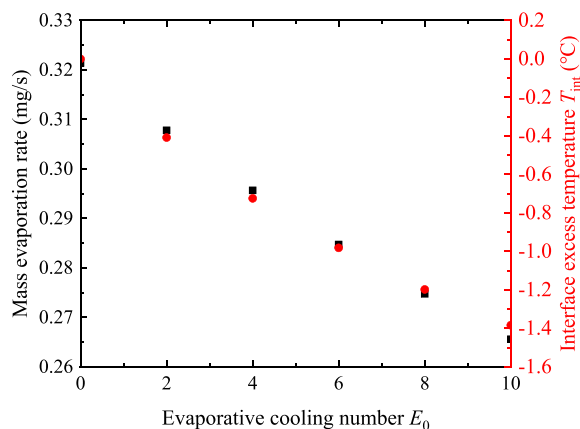


Figure 8. Changes in excess temperature at lens surface center and mass evaporation rate with evaporative cooling number E_0 when the ionic liquid temperature is 21 °C.

mass evaporation rate with evaporative cooling number E_0 when the ionic liquid temperature is 21 °C. Both the excess temperature at the lens surface center and the mass evaporation rate decrease with increasing evaporative cooling number E_0 ; that is, the evaporation process of the lens is inhibited.

CONCLUSIONS

In this study, a theoretical heat and mass transfer model of volatile liquid lenses evaporation on the immiscible liquid substrate surface is established in a toroidal coordinate system. According to the coupled boundary conditions based on the heat and mass transfer relationship at the gas–liquid interface as well as the evaporative cooling effect, the analytical solutions of the temperature field inside the lens and the vapor concentration field around the lens are derived. The reliability of the theoretical model is verified by an experimental measurement of hexane lens evaporation on the ionic liquid surface. Compared with the isothermal model, the contact radius calculated by the present model agrees well with the experimental data, especially when the liquid substrate temperature is relatively high.

According to the analytical solution, the temperature distribution inside the lens is not uniform, which is similar to the temperature distribution when sessile droplet evaporation on the surface of the solid substrate. The lowest temperature appears at the symmetry axis of the lens surface. Additionally, the excess temperature, heat flux, and evaporation flux at the lens–air interface increase monotonically from the lens center to the contact line. As liquid substrate temperature increases, the heat flux and evaporation flux increase accordingly, while the excess temperature decreases at the center of the lens surface. Finally, the effects of the density

ratio ($\rho_{\text{lens}}/\rho_{\text{substrate}}$) and evaporative cooling number (E_0) on the lens mass evaporation rate are analyzed. The results show that the lens mass evaporation rate decreases with increasing density ratio and evaporative cooling number.

ASSOCIATED CONTENT

Supporting Information

The Supporting Information is available free of charge at <https://pubs.acs.org/doi/10.1021/acsomega.2c00691>.

Toroidal coordinate system; governing equations and analytical solutions for the temperature field inside the lens; governing equations and analytical solutions for the vapor concentration field around the lens (PDF)

AUTHOR INFORMATION

Corresponding Author

Lu Liu – Department of Power Engineering and Hebei Key Laboratory of Low Carbon and High Efficiency Power Generation Technology, North China Electric Power University, Baoding 071003, China; orcid.org/0000-0002-2857-8491; Email: luliu@ncepu.edu.cn

Authors

Menglong Mi – Department of Power Engineering, North China Electric Power University, Baoding 071003, China
 Jian Jiang – Department of Power Engineering, North China Electric Power University, Baoding 071003, China
 Shulei Zhang – Department of Power Engineering, North China Electric Power University, Baoding 071003, China
 Xinyu Dong – Department of Power Engineering and Hebei Key Laboratory of Low Carbon and High Efficiency Power Generation Technology, North China Electric Power University, Baoding 071003, China

Complete contact information is available at: <https://pubs.acs.org/10.1021/acsomega.2c00691>

Notes

The authors declare no competing financial interest.

ACKNOWLEDGMENTS

This study was financially supported by the National Natural Science Foundation of China (51876065) and the Natural Science Foundation of Hebei Province of China (No. E2019502183).

REFERENCES

- (1) Erbil, H. Y. Evaporation of pure liquid sessile and spherical suspended drops: A review. *Adv. Colloid Interface Sci.* **2012**, *170*, 67–86.
- (2) Zang, D.; Tarafdar, S.; Tarasevich, Y. Y.; Dutta Choudhury, M.; Dutta, T. Evaporation of a droplet: from physics to applications. *Phys. Rep.* **2019**, *804*, 1–56.
- (3) Amjad, M.; Yang, Y.; Raza, G.; Gao, H.; Zhang, J.; Zhou, L. P.; Du, X. Z.; Wen, D. S. Deposition pattern and tracer particle motion of evaporating multi-component sessile droplets. *J. Colloid Interface Sci.* **2017**, *506*, 83–92.
- (4) Wang, C.; Xu, R. N.; Song, Y.; Jiang, P. X. Study on water droplet flash evaporation in vacuum spray cooling. *Int. J. Heat Mass Transfer* **2017**, *112*, 279–288.
- (5) Park, J.; Moon, J. Control of colloidal particle deposit patterns within picoliter droplets ejected by ink-jet printing. *Langmuir* **2006**, *22*, 3506–3513.
- (6) Dugas, V.; Broutin, J.; Souteyrand, E. Droplet evaporation study applied to DNA chip manufacturing. *Langmuir* **2005**, *21*, 9130–9136.

- (7) Picknett, R. G.; Bexon, R. The evaporation of sessile or pendant drops in still air. *J. Colloid Interface Sci.* **1977**, *61*, 336–350.
- (8) Deegan, R. D. Pattern formation in drying drops. *Phys. Rev. E: Stat. Phys., Plasmas, Fluids, Relat. Interdiscip. Top.* **2000**, *61*, 475–485.
- (9) Deegan, R. D.; Bakajin, O.; Dupont, T. F.; Huber, G.; Nagel, S. R.; Witten, T. A. Contact line deposits in an evaporating drop. *Phys. Rev. E: Stat. Phys., Plasmas, Fluids, Relat. Interdiscip. Top.* **2000**, *62*, 756–765.
- (10) Hu, H.; Larson, R. G. Analysis of the microfluid flow in an evaporating sessile droplet. *Langmuir* **2005**, *21*, 3963–3971.
- (11) Hu, H.; Larson, R. G. Marangoni effect reverses coffee-ring depositions. *J. Phys. Chem. B* **2006**, *110*, 7090–7094.
- (12) Erbil, H. Y.; McHale, G.; Newton, M. I. Drop evaporation on solid surfaces: constant contact angle mode. *Langmuir* **2002**, *18*, 2636–2641.
- (13) Guan, J. H.; Wells, G. G.; Xu, B.; McHale, G.; Wood, D.; Martin, J.; Stuart-Cole, S. Evaporation of sessile droplets on slippery liquid-infused porous surfaces (SLIPS). *Langmuir* **2015**, *31*, 11781–11789.
- (14) Armstrong, S.; McHale, G.; Ledesma-Aguilar, R.; Wells, G. G. Evaporation and electrowetting of sessile droplets on slippery liquid-like surfaces and slippery liquid-infused porous surfaces (SLIPS). *Langmuir* **2020**, *36*, 11332–11340.
- (15) Liu, L.; Xu, C.; Zhao, L. T.; Mi, M. L.; Li, C. X. Experimental and theoretical study of evaporation of a volatile liquid lens on an immiscible liquid surface. *Langmuir* **2019**, *35*, 12979–12985.
- (16) Liu, L.; Xu, C.; Zhu, M.; Jiang, J.; Mi, M. L. A study of the evaporation of hexane lenses on an ionic liquid surface: Effect of wetting mode. *Langmuir* **2020**, *36*, 1437–1445.
- (17) Liu, L.; Jiang, J.; Zhang, S. L.; Zhu, M.; Dong, X. Y.; Mi, M. L. Morphology evolution of a volatile liquid lens on another immiscible liquid surface induced by evaporation. *Langmuir* **2021**, *37*, 14081–14088.
- (18) Dash, S.; Garimella, S. V. Droplet evaporation dynamics on a superhydrophobic surface with negligible hysteresis. *Langmuir* **2013**, *29*, 10785–10795.
- (19) Xu, X. F.; Ma, L. R. Analysis of the effects of evaporative cooling on the evaporation of liquid droplets using a combined field approach. *Sci. Rep.* **2015**, *5*, No. 8614.
- (20) Chandramohan, A.; Weibel, J. A.; Garimella, S. V. Spatiotemporal infrared measurement of interface temperatures during water droplet evaporation on a nonwetting substrate. *Appl. Phys. Lett.* **2017**, *110*, No. 041605.
- (21) Nguyen, T. A. H.; Biggs, S. R.; Nguyen, A. V. Analytical model for diffusive evaporation of sessile droplets coupled with interfacial cooling effect. *Langmuir* **2018**, *34*, 6955–6962.
- (22) Shen, Y.; Cheng, Y. P.; Xu, J. L.; Zhang, K.; Sui, Y. Theoretical analysis of a sessile evaporating droplet on a curved substrate with an interfacial cooling effect. *Langmuir* **2020**, *36*, 5618–5625.
- (23) Das, S.; Dey, A.; Reddy, G.; Sarma, D. D. Suppression of the coffee-ring effect and evaporation-driven disorder to order transition in colloidal droplets. *J. Phys. Chem. Lett.* **2017**, *8*, 4704–4709.
- (24) Li, W. B.; Ji, W. J.; Lan, D.; Wang, Y. R. Self-assembly of ordered microparticle monolayers from drying a droplet on a liquid substrate. *J. Phys. Chem. Lett.* **2019**, *10*, 6184–6188.
- (25) Hakimian, A.; Mohebinia, M.; Nazari, M.; Davoodabadi, A.; Nazifi, S.; Huang, Z.; Bao, J.; Ghasemi, H. Freezing of few nanometers water droplets. *Nat. Commun.* **2021**, *12*, 6973.
- (26) Nosoko, T.; Ohyama, T.; Mori, Y. H. Evaporation of volatile-liquid lenses floating on an immiscible-liquid surface: effects of the surface age and fluid purities in n-pentane/water system. *J. Fluid Mech.* **1985**, *161*, 329–346.
- (27) Sun, W.; Yang, F. Q. Evaporation of a volatile liquid lens on the surface of an immiscible liquid. *Langmuir* **2016**, *32*, 6058–6067.
- (28) Wang, T. S.; Shi, W. Y. Marangoni convection instability in an evaporating droplet deposited on volatile liquid layer. *Int. J. Heat Mass Transfer* **2021**, *171*, 121055–121065.
- (29) George, D.; Damodara, S.; Iqbal, R.; Sen, A. K. Flotation of denser liquid drops on lighter liquids in non-neumann condition: Role of line tension. *Langmuir* **2016**, *32*, 10276–10283.
- (30) Lebedev, N. N. *Special Functions and Their Applications*; Prentice-Hall: Englewood Cliffs, NJ, 1965.